Marine precipitation has been observed by previous space-borne X-SARs. Because it appears to be difficult to separate the effects of downbursts, wind roughening and rain impact on the sea surfaces from signals produced by hydrometeors, the retrieval of maritime rainfall may be deferred until it has been demonstrated the utility of terrestrial precipitation retrievals.

In this work we approach the problem of X-SAR rain retrieval by showing some past experimental evidences and proposing a simple preliminary model to interpret X-SAR data.

2. Characteristics of future spaceborne SAR at X band

The TRMM was launched in November of 1997. It carried a 14-GHz Precipitation Radar (PR) that has a 200 km wide swath consisting of 50 cross track scanned ~ 4 km wide footprints. The PR also has 250 m vertical range resolution. Unlike the excellent vertical resolution provided by the PR, X-SARs yield data that consist of integrals of attenuation along and backscattering perpendicular to the viewing direction. Being path integrated quantities, X-SAR rainfall retrievals will be somewhat similar to microwave radiometric rainfall retrievals from a mathematical perspective.

1.1 *TerraSAR X (TSX)*

The forthcoming launch of the TSX space-based X-Band SAR could provide valuable precipitation observations during the latter part of the decade. The most significant features of TSX are that it operates at 9.7 GHz at HH,VH,HV and VV polarization with a PRF between 3 and 6.5 kHz. In a SCANSAR mode, TSX has a swath width of ~100 km with resolution of ~ 16 m. (While the swath width is less desirable than that of the PR, the higher spatial resolution opens new research opportunities) The subsequent lauch of TanDEM-X in 2008 will yield interferometric data that can be used to study motion fields. This feature may be useful for the study of cloud dynamics. TSX will be in an ascending orbit at ~18:00 local time. It will thus pass over the earth at nearly the same time as the US DoD DMSP F-13 satellite that carries a Scanning Sensor Microwave/ Imager (SSM/I) in an orbit that crosses the equator in a northward direction at 17:43 local time. The NOAA-15 satellite carries Advanced Microwave Sounding Units (AMSU-A&B). That satellite crosses the equator in a northward direction at 19:00 local time. The Coriolis satellite, which carries multi frequency radiometers that measure all four Stoke's vectors between 6.8 and 37.0 GHz, also crosses the equator in a northward direction at ~18:00. These sensors, which straddle the proposed TSX orbit, could provide ancillary microwave measurements, albeit with poorer spatial resolution.

1.2 *COSMO-SkyMed (CSM)*

The COSMO-SkyMed will consist of four satellites and will operate at 9.6 GHz with selectable polarizations, HH, VV, HV, and VV. It will fly in a polar orbit and the orbital plane and equator crossing times will be around 0600 local time, nearly the same as TSX, but in the opposite direction. Tropical precipitation events may thus be viewed by both X-SARS. In a SCANSAR mode, COSMO-SkyMed has a swath width of 200 km with resolution of 100 m. Because COSMO-SkyMed will consist of several X-SARs, it will also have interferometric capability. Complementary visible observations will be available from two French PLEIADES satellites that will fly in the same orbital plane as COSMO-SkyMed. Data may be obtained from other satellites as they enter service. The dual polarization capabilities of TSX and COSMO-SkyMed will be beneficial to discriminate between wet ground and warm rain. Because precipitating systems contain liquid as well as dry frozen hydrometeors and supercooled water, measuring the full scattering matrix, the DPPS and perhaps supplemental data from passive microwave radiometers should provide useful information about the hydrometeors. Interferometric data from TanDEM-X and COSMO-SkyMed could provide further constraints on precipitation retrievals.

3. Precipitation observations from X-SAR Data

C-band and L-band SARs have a long heritage of Earth observation (Moore et al., 1997; Melsheimer et al., 1998 and 2001).

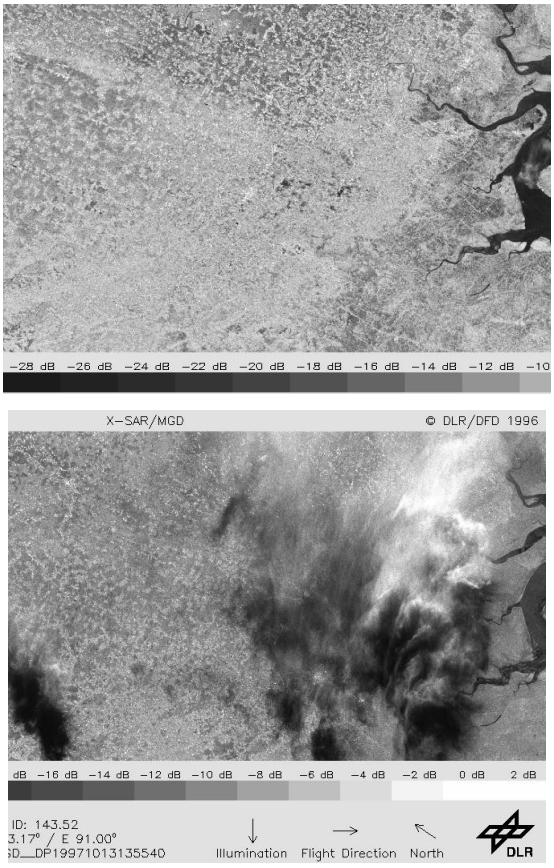

Fig. 1. (Upper) View of Calcutta (22.8ºN x 91.2ºE) on 7 October, 1994. (Lower) Same scene on 18 April, 1994. Note scattering by frozen hydrometeors in the upper right, scattering and attenuation by rain in middle-lower right, and possible absorption by rain only in the lower left. The maximum NRCS of the scattered signal is ~ -3 dB and the minimum NRCS value in the shaded area is ~ -30 dB.

Those studies showed that X-SARs are more sensitive to rainfall effects than SARs operating at longer wavelengths because the rainfall reflectivity at X-band is enhanced by ~ 12 dB and the attenuation increases by ~ 4 dB as compared to C-band reflectivities and attenuation. The Shuttle Missions STS-59 and 68 of 1994 carried an X- SAR from DLR along with L and C band SARs provided by JPL. The X-SAR had a ~ < 50 km wide swath width with ~0.6 km resolution, and it could observe precipitation. The X-SAR only measured VV polarization.

The sensitivity to scattering by precipitation can be seen in Fig. 1 showing X-SAR images obtained over Calcutta, India in 1994. The upper part of Fig. 1 (upper) shows a scene without precipitation. The lower image shows a convective rainy system on the same geographical area. Note that a "plume" appears to be sheared eastward. The Doppler spread caused by turbulence within the cloud may degrade the cross-track resolution to ~ 0.5 km so that some streakiness perpendicular to the satellite orbit may be expected, Atlas and Moore (1987). However, the streakiness of the enhanced NRCS is canted with respect to the cross-track direction. This suggests that although the Doppler effect, caused by turbulence, may contribute to this streakiness, but the appearance of that precipitation may also be due to the vertical distribution of the frozen hydrometeors. X-SAR data modeling efforts suggest that the wisps may be the horizontal projections of obliquely viewed frozen hydrometeor columns. Note that, because this is an X-band image, this is not a simple cirrus anvil and that the frozen particles are snow or graupel. The lower left hand part of the image shows a dark region with negligible brightening near the leading edge. This suggests the presence of shallow rain that scatters little radiation, yet rain attenuates radiation on its way to and from the surface. However, it is possible that this effect may be caused by surface wetting from antecedent rainfall. Dual polarized data from the forthcoming X-SARs, could resolve this issue.

4. Modeling of X-SAR data due to rainfall

The measured NRCS (Normalized Radar Cross Section) signal σ_{SAR} consists of two components, the scattering from the surface, σ_{1srf}, and scattering by the precipitation, σ_{2vol}, such that:

$$\sigma_{SAR} = \sigma_{1srf} + \sigma_{2vol} \tag{1a}$$

We have developed a simple numerical model of the NRCS from a horizontally finite cloud that consists of layers of rain and frozen hydrometeors (Weinman, 2006). The model is schematically depicted in **Fig.2**. If σ_0 is the surface NCRS, the constituents of Eq. (1a) are:

$$\sigma_{1srf} = \sigma_0 \left(\frac{\Delta}{\sin\theta} \right) e^{-2\int_0^{\infty} k[x(z)] \frac{dz}{\cos\theta}} \tag{1b}$$

$$\sigma_{2vol} = \sigma_0 \left(\frac{2\pi\Delta}{\sin\theta} \right) \int_0^{\infty} \eta[x(z)] e^{-2\int_0^{\infty} k[x'(z')] \frac{dz'}{\cos\theta}} \frac{dz}{\cos\theta} \tag{1c}$$

where the radar reflectivity (or volume scattering coefficient) is η [km^{-1}] and the extinction coefficient is k [km^{-1}]. The horizontal and vertical coordinates are x and z respectively. The scattering volume occurs within a slice of oblique thickness Δ/2 in the direction of propagation and θ is the angle from nadir. Numerous types of hydrometeors may occur in precipitating clouds, and they contribute differently to η and *k*.

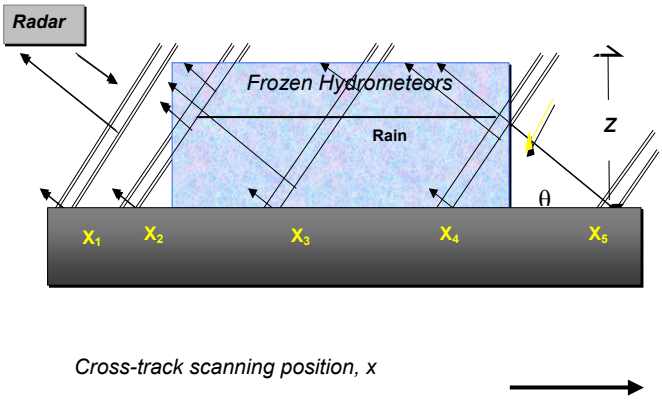

Fig. 2. Schematic view of the NRCS reflectivity model.

As we move from left , x_1, to right, x_5, the first slice consists of unattenuated returns from the surface, the second consists of unattenuated scattering from the surface and attenuated scattering from the frozen hydrometeors at the top of the cloud. As we move further to the right, x_3 , all components contribute to the NRCS. At x_4, the surface scattering is attenuated by the rain, but there is less scattering by the frozen hydrometeors. Finally, as we approach x_5 on the far right side of the figure, only the attenuated surface reflection contributes to the NRCS.

The radar model here employed has features similar to those considered by Moore et al. (1997). However, our model can accommodate various distributions of hydrometeor scattering and attenuation properties within the cloud (Weinman, 2006). Fig. 3 shows examples of the X-band scattering properties of heavy rain and graupel and small hail derived from the modeling work of Marzano et al. (2006).

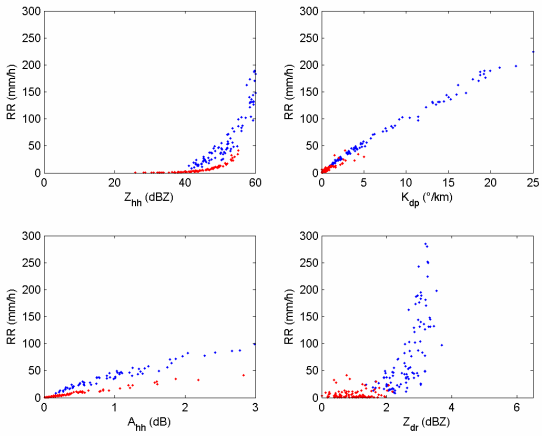

Fig. 3. Examples of the X-band hydrometeor parameters for horizontal polarization reflectivity (upper left), the differential phase shift (°/km) (upper right , the one-way co-polar attenuation (dB/km) (lower left), and the differential reflectivity (lower right), for graupel (red) and rain (blue).

Fig. 4 shows four sample vertical distributions of rain rates (mm/h) for four 6 km wide model clouds. One has a 32 mm/h surface rain rate. Two cloud models have 96 mm/h surface rain rates, but with differing amounts and vertical distributions of snow in the upper parts of the cloud. Those profiles were derived from isopleths of frequencies of attenuation corrected effective radar reflectivity factors, dBZeff , displayed as Contoured Frequency by Altitude Diagrams (CFAD) for convective storms obtained from TRMM PR measurements over eastern India .

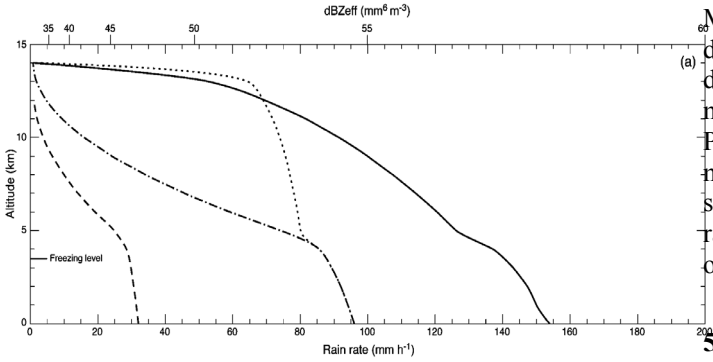

Fig. 4. Profiles of rain rates (mm/h) used to compute the NRCS model results shown in Fig. 5. The dash-dot Curve 1 is a profile with 32 mm/.h surface rainfall and light snow content, the dashed Curve 2 is a profile with surfae rainfall of 96 mm/h and modest snow content and the dotted Curve 3 is similar to curve 2, but with more snow.

The NRCSs, derived from these models, are shown in Fig. 5. The horizontal location of the cloud is shown as the 6 km wide shaded zone. The increase of the NRCS to the left of the cloud, from -7 dB to about -4 dB is proportional to the ice content. An empirical fit to data from several such cloud models yields:

$$R(z = 8km) \cong 1.1 \cdot 10^4 \, Max[\sigma_{SAR}]^5 \pm 20\% \qquad (2a)$$

for the melted rainfall rate *R(z=8km)* [mm/h] at a height of 8 km as a function of the maximum value of the NRCS.

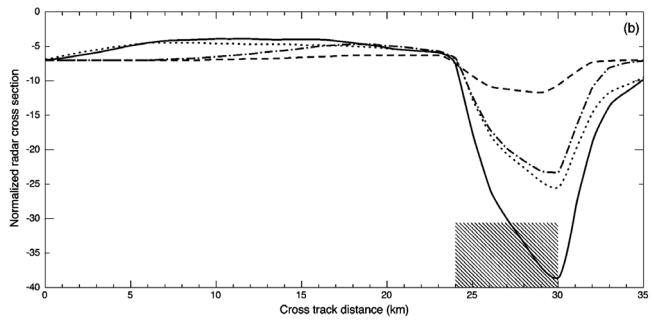

Fig. 5. Distributions of NRCS values perpendicular to the satellite orbit computed from the NRCS model profiles shown in Fig. 3. The curves use the same line classification shown in Fig. 3. The precipitating cloud is located in the shaded area.

Although the long gradual rise of the NRCS to the left of the cloud appears as if it was a sheared plume emanating from the cloud top, it is just a characteristic of the scattering mechanism. The length, ℓ, of that "plume" is proportional to the height, h, of the frozen hydrometeor cloud, i.e.:

$$\ell \cong h / \tan(\theta) \qquad (2b)$$

The minimum NRCS values that ranged from ~ -12 to ~ -40 dB depended mainly on the rain content and a provisional relationship can be developed for the surface rain rate *R(z=0km)* [mm/h]:

$$R(z = 0km) \cong 20 Min[\sigma_{SAR}]^{-0.25} \pm 20\% \qquad (2c)$$

These preliminary findings suggest that some information about precipitation profiles may be retrieved from NRCSs. More work is needed and our proposed activities are described below. The availability of HH and VV polarized data from TSX and COSMO-SkyMed will permit the measurement of dual polarized NRCS and the differential Propagation Phase Shift (DPPS). Because rain drops become more aspherical as they enlarge, Jameson (1991) was able to show that such measurements could be related to rainfall rates. The DPPS has been used as a constraint on retrievals of specific attenuation profiles by Vulpiani et al. (2005).

5. Conclusions

This investigation is a preliminary study aimed to: i) define a numerical NRCS rain cloud model to accommodate various distributions of liquid, melting and frozen hydrometeors. ii) establish an inversion scheme based on a Bayesian or a neural-network approach, exploiting what already done for satellite microwave radiometry of rainfall using a Monte Carlo approach and cloud-resolving model simulations. The presented results seem to be promising even though a deeper analysis is needed to resolve ambiguities in the X_SAR rain signatures. A validation activity of rainfall SAR-retrieval over land should be also foreseen by using ground-based C-band meteorological radar networks.

References

Atlas, D., R.K. Moore, 1987, The measurement of precipitation with synthetic aperture radar. *J. Atmos. and Ocean Tech*., **4**, 368-376.

Jameson, A.R., 1991: A comparison of microwave techniques for measuring rainfall. *J. Appl. Met*., **30**, 32-54.

Marzano, F.S., D. Scaranari, M. Celano, P.P. Alberoni, G. Vulpani, M. Montopoli, 2006, Hydrometeor classification fromdual-polarized weather radar: extending fuzzy logic from S-band to C-band data, *Advances in Geosci*., **7**, 109-114.

Melsheimer, C., M. Gade, and W. Alpers, 1998, Investigation of multifrequency/multipolarization radar signatures of rain cells derived from SIR-C/X-SAR data, *J. Geophys. Res*., **103**, 18,867-18,884.

Moore, R. K., A. Mogili, Y. Fang, B. Beh, A. Ahamad, 1997, Rain measurement with SIR-C/X-SAR," *Remote Sensing of Environment*, **59**, 280-293.

Weinman, J.A., 2006, Precipitation Measurement with X-band Synthetic Aperture Radar, NASA proposal for INSPIRES Call, April 10.

Vulpiani G., F.S. Marzano, V. Chandrasekar and S. Lim, 2005: Constrained Iterative Technique with Embedded Neural-Network for Dual-Polarization Radar Correction of Rain Path Attenuation, *IEEE Trans. Geosci. Rem. Sensing*, **43**, 2305-2314.